A frequency-based analysis of cutting force for depths of cut identification in peripheral end-milling

A frequency-based analysis of cutting force for depths of cut identification in peripheral end-milling

Niccolò Grossi, Lorenzo Morelli, Antonio Scippa, Gianni Campatelli

PII: S088832702200125X

DOI: 10.1016/j.ymssp.2022.108943

To appear in: *Mechanical Systems and Signal Processing*

Received Date: 30 September 2021

Revision Date: 18 January 2022

Accepted Date: 7 February 2022

Please cite this article as: Grossi N, Morelli L, Scippa A, Campatelli G (2022) A frequency-based analysis of cutting force for depths of cut identification in peripheral end-milling. Mech Syst Signal Process 171:108943, https://doi.org/10.1016/j.ymssp.2022.108943

Title

A frequency-based analysis of cutting force for depths of cut identification in peripheral end-milling

Authors

Niccolò Grossi[a,*], Lorenzo Morelli[a], Antonio Scippa[a], Gianni Campatelli[a]

[a]Department of Industrial Engineering, University of Firenze, via di Santa Marta 3, 50139, Firenze, Italy.

*corresponding author. Tel. +390552758726. E-mail: niccolo.grossi@unifi.it

Abstract

This paper presents a novel approach to identify both radial and axial depth of cut in 2.5-axis peripheral milling operations using cutting force signals analysed in the frequency domain (i.e., cutting force spectrum). In detail, the method exploits the normalized cutting force spectrum, which is directly obtained through dedicated analytical formulations, to estimate depths of cut. The proposed approach is promising and differs from previous works since it does require nor the cutting force coefficients or cutting force direction neither a dedicated instrumentation. The developed method was numerically and experimentally validated in different cutting conditions. The results obtained show that depths of cut are identifiable with a maximum absolute error less than 0.4 mm, proving that the proposed approach could be a solid foundation for a force based cutting condition monitoring system in peripheral milling.

Keywords: End milling; Simulation; Frequency; Cutting Force; Monitoring.

1. INTRODUCTION

In the context of smart manufacturing, monitoring and control have become fundamental elements to increase the productivity and quality of industrial processes [1]. Focusing on machining, quality and productivity of cutting operations are strictly related to the parameters adopted, therefore, knowing and measuring such parameters during the process is essential to support any control or monitoring strategy [2]. In peripheral milling, some of these parameters, such as spindle speed and feed, are already monitored and regulated through the numerical control of the machine tool, however no solution for measuring and monitoring the engagement parameters (i.e., radial and axial depths of cut) is generally available. Nonetheless, the identification of the engagement conditions during the cutting process could allow process faults, such as tool collision or mistakes in toolpath programming, to be detected and avoided. In literature, several methods that aim at identifying the engagement parameters, have been presented. Most of them are based on the comparison between simulated and measured cutting forces, which represent a variable directly related to the cutting conditions. To develop such methods, it is hence required both measurements and modeling of cutting forces.

On one hand, several techniques are available for cutting force measurement in milling operations. For example, piezo-electric dynamometers are commercially adopted for cutting force measurements in milling [3]. However, they are expensive, and they affect the dynamic of the cut by changing the mass and the stiffness of the machine tool. As well as this, the dynamic of table dynamometers is related to the size of the workpiece, generally limiting their use to small components, while rotating dynamometers suffers from low flexibility and reconfigurability. Other force measurement tools are the ones that use spindle and feed drive current signals, and indirectly measure the cutting forces [4]. Such methods are accurate, but their range of application is restrained by the bandwidth of the spindle and feed drive system. For these reasons, complex compensation strategies [5,6] are essential for an accurate force measurement. On the other hand, force measurements based on accelerometer signals are also available [7]. These methods need the direct measurement of the frequency response functions (FRFs) between the tool nose and the spindle box where the accelerometers are mounted. Furthermore, methods based on multiple sensors and fusion schemes have been presented [8,9]. These methods aim at overcoming the limitations of the previously mentioned techniques, but they still require FRFs measurements as input. In general, milling cutting forces can be accurately measured

with commercial sensors if a calibration phase is performed and an adequate post-processing strategy to compensate for dynamics of the system is performed.

On the other hand, the accuracy of the cutting model is critical for a good comparison between measured and predicted signals [10]. In this context, cutting forces in peripheral milling are widely represented through mechanistic models, which considers that the instantaneous cutting force is proportional to the uncut chip area through cutting coefficients [11]. Such cutting coefficients depend on the tool edge geometry and the tool/workpiece material properties [12]. Moreover, mechanistic force models may assume two different expressions: the first one, which includes one single coefficient (i.e., lumped shear force model) and the second one, which considers two separate coefficients (i.e., dual-mechanism force model). In the lumped shear force model [13], the single coefficient (i.e., cutting coefficient) gathers the effects of both shearing and ploughing leading to a simplified force representation with limited accuracy in a wide range of cutting parameters. On the other hand, the dual mechanism force model is more complex, and it presents one coefficient to evaluate the effects of shearing (i.e., cutting coefficient) and another coefficient to analyze the effects of ploughing (i.e., edge coefficient) allowing the cutting force representation to be more accurate in a broad range of cutting parameters [14]. However, the quantitative reliability of the cutting model depends on the accuracy of cutting force coefficients [15], and edge coefficients depend also on tool wear and surface inclination, as shown by Wojciechowski et al [16]. For that reason the lumped shear force model still represents an interesting choice since it has the advantage to rely on a single coefficient and is found to be accurate if its coefficients are computed and used in a small range of cutting parameters [17].

Based on these two components (i.e., cutting force modeling and measurement), Altintas et al. [18] developed an algorithm to identify of both axial depth and radial width of cut based only on two orthogonal force measurements in the plane perpendicular to the machine tool spindle using a table dynamometer. The algorithm evaluated the depths of cut with a maximum error less than 10%, and it was based on a mechanistic representation of the cutting forces, but it required calibration tests to identify the constants in the force equations. On the other hand, Choi et al. [19] proposed an algorithm to evaluate the axial depth of cut based on the pattern of cutting force without requiring the magnitude of the cutting force itself. The authors adopted a mechanistic cutting force model to identify the angular position where cutting force starts rising and the angular position where cutting force starts decreasing, then the angular distance between these two positions was used to obtain the axial depth of cut. However, the effect of the number of flutes cutting simultaneously on cutting force pattern was not fully investigated by the authors, limiting the reliability of the method. Moreover, cutting constants are still needed for the depths of cut identification. Yang et al. [20] analyzing the resultant cutting force shape with a mechanistic cutting model presented analytical force indices to correlate the depths of cut variations with force shape. The method proposed by authors extends the cutting force pattern results presented in the previous study, and it gives a maximum error less than 3% in the estimation of the depths of cut changes. However, both cutting coefficients and nominal values of depths of cut must be known to evaluate their deviations. Leal-Munoz et al. [21] presented an online approach to identify both axial and radial depths of cut from the cutting force pattern signal in finishing operations with tool runout. In detail, the authors evaluated the radial and axial depths of cut from the instant corresponding to the beginning of the cut and the axial depth of cut from the instant corresponding to the end of the cut. In this case the results obtained by the authors were extremely accurate with a relative error under 3%, but the approach applies only to cutting operations where only one flute is involved in the process and high axial depths of cut are adopted. The same authors [22] perfected their methods by considering the impact of the depths of cut and the spindle speed on the instant corresponding to the end of the cut, reaching a maximum error less than 0.05 mm in depths of cut measurements. Despite the increased accuracy, the limitations previously described remain.

Alternatively, depths of cut identification techniques based on specific instrumentations have been presented. Prickett et al. [23] proposed a methodology to provide real-time representation of the axial

depth of cut during end milling operation. The authors adopted two ultrasonic analogue distance sensors mounted on both sides of the tool to measure the distance of the workpiece in front of the cutter path and behind the cutter path. Then, the axial depth of cut was evaluated as the difference between the two measured distances. This method provided accurate results with a maximum error of 0.2 mm, however only small values of axial depth of cut were tested, and the radial depth of cut was not included. On the other hand, Gaja et al. [24] proposed a monitoring system to detect the axial depth of cut in real time using an acoustic emission (AE) sensor and a prediction model. In detail, the authors used a regression model to relate the AE signal and the axial engagement, and then they built an artificial neural network (ANN) for more accurate estimation of the axial depth of cut. The approach showed good results, but it requires a large amount of data, and it does not include the radial depth of cut. The mentioned approaches do not exploit any previous knowledge about the cutting process, they focus only on the axial depth of cut, and they require additional components and sensors which the machine tool must be adapted for, limiting their industrial application.

This paper presents a novel approach to identify both radial and axial depth of cut in 2.5-axis peripheral milling operations using cutting force signal analysed in the frequency domain (i.e., cutting force spectrum). Compared to the methods based on specific instrumentation, the proposed approach estimates both the depths of cut and does not require additional sensors or equipment, except for the one required to measure cutting forces. On the other hand, the method shares with other approaches the exploitation of cutting force measurement and the comparison with simulated results, but it does not perform such tasks in time-domain, as most of the proposed methods, but in frequency domain. Very few approaches adopt the cutting force analysis in the frequency domain for monitoring purposes. For example, Wang et al. [25] applied the convolution analysis to a mechanistic cutting force model to develop closed form expression of the cutting force in the frequency domain (i.e., force spectrum). As well as this, the same authors exploited the formulations developed to identify the cutter offset [26] and the cutting coefficients [17]. These approaches rely on the cutting force magnitude spectrum which requires the information about cutting force coefficients. This paper, starting from the cutting force representation as a Fourier series, as in [27] and [28], proposes new formulations to express the Fourier coefficients that describes the cutting force spectrum (i.e., resultant of radial and tangential cutting forces), improving their efficiency compared to the previous work [28]. Moreover, these formulations are exploited to identify the radial and axial depths of cut in peripheral 2.5 milling operations. In detail, the proposed approach uses the cutting force spectrum normalized to the zero-frequency component (i.e., mean value). The main advantages of the proposed approach are: i) the fast estimation of depths of cut since the comparison is performed on few values (tooth pass frequency and harmonics), suitable for a future real-time application iii) not requiring cutting force coefficients, cutting direction and tool run-out estimation, iv) not requiring specific instrumentation or sensors. The proposed approach was experimentally and numerically validated, and it proved to be a solid starting point for a force based cutting condition monitoring system.

2. PROPOSED MONITORING STRATEGY

In this work a novel monitoring solution for the identification of depths of cut (i.e., radial and axial) in end-milling is proposed. As general rule, an efficient monitoring system based on cutting force measurement should be able to analyze the process with the following features:

- Requiring the smallest number of parameters, and only the ones known by the operator;
- Not requiring information about cutting force model (e.g., cutting force coefficients);
- Not requiring information about cutting direction.

To achieve such ambitious goal, the idea presented in this work is to adopt total cutting force on x-y plane that can be computed as:

$$F_{tot}(\phi) = \sqrt{F_t^2(\phi) + F_r^2(\phi)} = \sqrt{F_x^2(\phi) + F_y^2(\phi)} \quad (1)$$

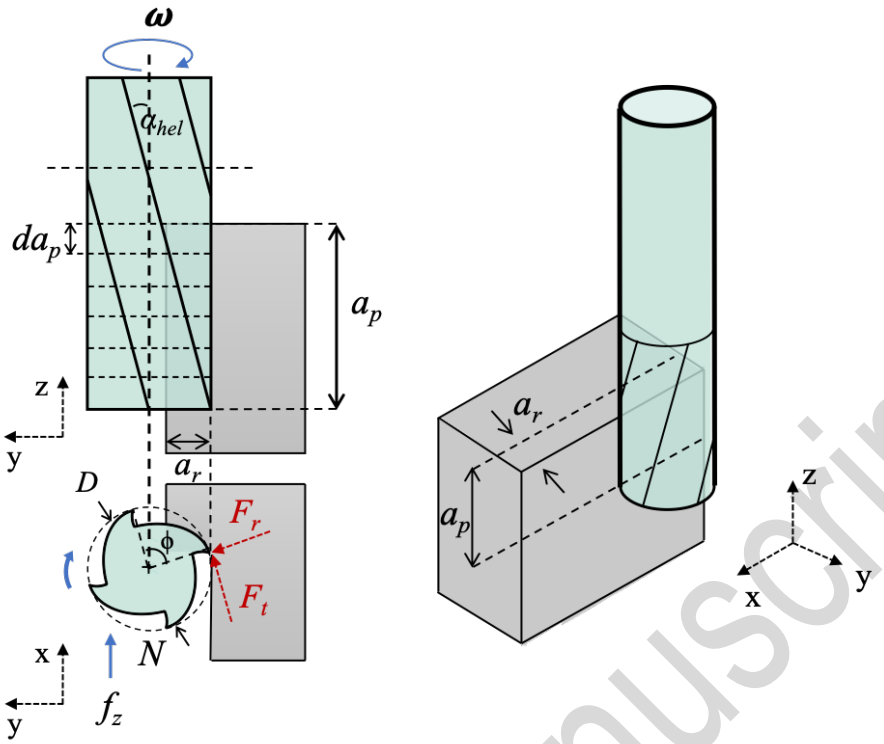

Fig. 1 Cutting tool and cutting parameters

where F_t and F_r are the forces on tangential, radial directions respectively (Fig. 1), while F_x and F_y are the cutting force on feed and cross-feed directions. However, this total force can be obtained by combining any couple of orthogonal forces on the x-y plane, therefore it can be easily acquired during the end-milling process without the need of the cutter direction.

To achieve the other features, the proposed strategy is based on the analysis of total cutting force signal in frequency domain, and depths of cut are estimated by comparing such information with the results of the enhanced analytical formulations derived in this work.

The proposed approach follows these steps:

1) Cutting forces are acquired in time domain in different directions with adequate sampling frequency (to cover at least *c* times the tooth pass frequency); if it is required, a compensation of distortions derived by the measuring system dynamics should be performed on these signals.
2) x-y plane total force is computed using eq. 1 to remove the necessity to estimate cutting direction.
3) A procedure to remove the influence of run-out on the cutting force is applied, at the end of this procedure the averaged total cutting force on a single tooth pass interval is isolated.
4) Discrete Fast Fourier Transformation (DFFT) is performed on the signal, constant term A_{0m} and the tooth pass frequency and harmonics (C_{nm}) are isolated to compute R_{nm}.
5) An optimization algorithm is performed to estimate depths of cut, computing the R_{np} according to eq. 32 and minimizing the error function *fo*.

The details of the mathematical formulations and procedures required by the proposed approach are presented in the next sub-sections.

2.1 Cutting force frequency content

The proposed solution is based on analytical equations that predict frequency content of cutting forces. These proposed formulations are valid for 2.5-axis end-milling process and consider a simple mechanistic force model that relates forces linearly to chip thickness with a cutting force coefficient (lumped shear model), as adopted in other approaches (e.g., [29]). Focusing on tangential and radial forces (Fig. 1)., the resulting cutting forces in time-domain are:

$$F_t(\phi) = \sum_{j=1}^{N} K_{tc} a_p h(\phi_j) \quad (2)$$

$$F_r(\phi) = \sum_{j=1}^{N} K_{rc} a_p h(\phi_j) \quad (3)$$

where K_{tc}, K_{rc} are the tangential and radial cutting coefficients, N is the number of flutes, a_p is the axial depth of cut and h is the chip thickness that can be computed as:

$$h = f_z \sin(\phi_j) \quad (4)$$

where:

$$\phi = \omega t \quad (5)$$

$$\phi_j = \phi + \left(\frac{2\pi}{N}\right)(j-1) \;\; j = 1,2,\dots,N \quad (6)$$

where f_z is the feed per tooth, t is the time variable and ω is the spindle speed in rad/s (Fig. 1).
Such time-domain equations should be evaluated only in the range of cutter entry angle (ϕ_{in}) and cutter exit angle (ϕ_{out}) which are identified according to the cutting strategy and the radial depth of cut (a_r) with these expressions:

$$\phi_{in} = \pi - \alpha_{en} \textit{ Down-milling;} \qquad \phi_{in} = 0 \textit{ Up-milling} \quad (7)$$

$$\phi_{out} = \pi \textit{ Down-milling;} \qquad \phi_{out} = \alpha_{en} \textit{ Up-milling} \quad (8)$$

where D is the tool diameter and:

$$\alpha_{en} = \operatorname{acos}(2a_r/D) \quad (9)$$

Starting from this time-domain representation, it is possible to derive the expressions in frequency domain. The proposed approach starts from the formulation in frequency domain for F_y proposed by Schmitz et al. [28]:

$$F_y(\phi) = \sum_{j=1}^{N}(a_{y0} + \sum_{n=1}^{\infty}(a_{yn}\cos n\phi_j + b_{yn}\sin n\phi_j)) \quad (10)$$

where $a_{0\dots}$ a_n are the Fourier series terms that, for the purpose of this work, can be written as:

$$a_{y0} = a^*_{y0} \cdot a_p; \quad a_{yn} = a^*_{yn} \cdot a_p; \quad b_{yn} = b^*_{yn} \cdot a_p \quad (11)$$

where a^*_{y0} represents the Fourier coefficients at zero frequency, while a^*_{yn}, b^*_{yn} are two coefficients which define the real and imaginary components of force at the frequency n-multiple of the rotation frequency (n integer), divided for the axial depth of cut. This formulation was derived for F_y because the focus of Schmitz et al. work [28] was on surface error that is mainly caused by y-direction displacements, however for the purpose of this work, it can be easily demonstrated that the same formulation can be obtained for the cutting force on the x-y plane (F_{tot}) with different Fourier coefficients.

$$F_{tot}(\phi) = \sum_{j=1}^{N}(a^*_{tot0} \cdot a_p + \sum_{n=1}^{\infty}(a^*_{totn} \cdot a_p \cos n\phi_j + b^*_{totn} \cdot a_p \sin n\phi_j)) \quad (12)$$

The full expressions for a^*_{totn} and b^*_{totn} are reported in the Appendix A.
The force formulation in eq. 13 is valid in case of straight teeth cutting tool; however, to achieve an accurate force prediction it is necessary to include helix angle, therefore the equations are rearranged by including an additional summation, as proposed by Schmitz et al. [28]:

$$F_{tot}(\phi) = \sum_{k=1}^{A}\sum_{j=1}^{N}(a^*_{tot0} \cdot da_p + \sum_{n=1}^{\infty}(a^*_{totn} \cdot da_p \cos n(\phi_j - \psi\cdot(k-1)) + b^*_{totn} \cdot da_p \sin n(\phi_j - \psi\cdot(k-1)))) \quad (13)$$

To achieve the goal, the tool is discretized in A axial slices, each slice (da_p high) is assumed to have a zero helix angle and the slices are rotated relative to one another by the angle ψ:

$$\psi = k_b da_p \quad (14)$$

$$k_b = 2\tan(\alpha_{hel})/D \tag{15}$$

where α_{hel} is the helix angle. This assumption introduces an approximation that could lead to errors, especially increasing helix angle and reducing the number of slices. Moreover, an additional summation is included to the Fourier series, reducing the computational efficiency. In this work eq. 13 is rearranged to remove this summation and the related approximation, by introducing the integral:

$$F_{tot}(\phi) = \int_0^{a_p} \sum_{j=1}^{N} (a^*_{tot0} \cdot dx + \sum_{n=1}^{\infty} (a^*_{totn} \cdot dx \cos n(\phi_j - k_b x dx) + b^*_{totn} \cdot dx \sin n(\phi_j - k_b x dx))) \tag{16}$$

$$F_{tot}(\phi) = a^*_{tot0} \cdot N a_p + \sum_{j=1}^{N} \sum_{n=1}^{\infty} (\int_0^{a_p} (a^*_{totn} \cdot dx \cos(n\phi_j - n k_b x dx) + b^*_{totn} \cdot dx \sin(n\phi_j - n k_b x dx)) \tag{17}$$

The phase shift ($k_b x dx$) given by the helix angle can be rearranged by following simple trigonometric steps (angle sum and difference identities):

$$F_{tot}(\phi) = a^*_{x,y0} \cdot N a_p + \sum_{j=1}^{N} \sum_{n=1}^{\infty} \Big(\int_0^{a_p} (a^*_{totn} \cdot dx \cos n\phi_j \cos n k_b x dx + a^*_{totn} \cdot dx \sin n\phi_j \sin n k_b x dx + b^*_{totn} \cdot dx \sin n\phi_j \cos n k_b x dx - b^*_{totn} \cdot dx \sin n\phi_j \cos n k_b x dx) \Big) \tag{18}$$

$$F_{tot}(\phi) = a^*_{x,y0} \cdot N a_p + \sum_{j=1}^{N} \sum_{n=1}^{\infty} \Big(\int_0^{a_p} ((a^*_{totn} \cdot dx \cos n k_b x dx - b^*_{totn} \cdot dx \sin n k_b x dx) \cos n\phi_j + (a^*_{totn} \cdot dx \sin n k_b x dx + b^*_{totn} \cdot dx \cos n k_b x dx) \sin n\phi_j) \Big) \tag{19}$$

Solving the integral in eq. 14, the following equations can be derived:

$$F_{tot}(\phi) = a^*_{x,y0} \cdot N a_p + \sum_{j=1}^{N} \sum_{n=1}^{\infty} \Big[((\frac{a^*_{totn}}{n k_b} \sin n k_b x + \frac{b^*_{totn}}{n k_b} \cos n k_b x) \cos n\phi_j + (-\frac{a^*_{totn}}{n k_b} \cos n k_b x + \frac{b^*_{totn}}{n k_b} \sin n k_b x) \sin n\phi_j) \Big]_0^{a_p} \tag{20}$$

$$F_{tot}(\phi) = a^*_{x,y0} \cdot N a_p + \sum_{j=1}^{N} \sum_{n=1}^{\infty} \Big(((\frac{a^*_{totn}}{n k_b} \sin n k_b a_p + \frac{b^*_{totn}}{n k_b} \cos n k_b a_p - \frac{b^*_{totn}}{n k_b}) \cos n\phi_j + (-\frac{a^*_{totn}}{n k_b} \cos n k_b a_p + \frac{a^*_{totn}}{n k_b} + \frac{b^*_{totn}}{n k_b} \sin n k_b a_p) \sin n\phi_j) \Big) \tag{21}$$

The proposed formulations allow estimating cutting forces in the frequency domain in presence of helix angle using an exact expression, without the need of a specific discretization.

- For the constant term (null frequency):

$$a^*_{tot0} \cdot N a_p \tag{22}$$

- For tooth pass frequency and its harmonics:

$$\frac{1}{2} \sum_{j=1}^{N} \sum_{n=1}^{\infty} \Big(((\frac{a^*_{totn}}{n k_b} \sin n k_b a_p + \frac{b^*_{totn}}{n k_b} \cos n k_b a_p - \frac{b^*_{totn}}{n k_b}) \cos n\phi_j + (-\frac{a^*_{totn}}{n k_b} \cos n k_b a_p + \frac{a^*_{totn}}{n k_b} + \frac{b^*_{totn}}{n k_b} \sin n k_b a_p) \sin n\phi_j) \Big) \tag{23}$$

Moreover, it is interesting to point out that, similar to what is proposed for force shape characteristics [20], two main angles are responsible for the frequency content of the cutting forces:

- the radial engagement angle (α_{en}) responsible for ϕ_{in}-ϕ_{out} range that affects a^*_{totn} and b^*_{totn}.
- the axial engagement angle or sweep angle (α_{sw}) that depends on helix angle and axial depth of cut according with the following equation:

$$\alpha_{sw} = k_b a_p \tag{24}$$

It is worth mentioning that the proposed formulations derived in this work for total force (eq. 21) are valid also for cutting forces in different directions (e.g., x and y) and considering different cutting force models (e.g., including edge coefficients or run-out), indeed, in such cases, only Fourier coefficients are changing.

However, the proposed solution is based on total cutting force for the already mentioned feature to be independent on cutting direction, while a lumped shear cutting force model (eq. 2-3) is chosen because in this condition, cutting force coefficients can be easily isolated and the Fourier terms a^*_{totn} and b^*_{totn} can be written as:

$$a^*_{tot0} = a^{**}_{tot0} \cdot f_z\sqrt{{K_{tc}}^2 + {K_{rc}}^2} \quad (25)$$

$$a^*_{totn} = a^{**}_{totn} \cdot f_z\sqrt{{K_{tc}}^2 + {K_{rc}}^2} \quad (26)$$

$$b^*_{ton} = b^{**}_{totn} \cdot f_z\sqrt{{K_{tc}}^2 + {K_{rc}}^2} \quad (27)$$

where a^{**}_{totn} and b^{**}_{totn} depend only on radial depth of cut and their full expressions are reported in the Appendix A. Using expressions in eq. 25-27, eq. 21 can be re-arranged as:

$$F_{tot}(\phi) = a^{**}_{tot0} \cdot f_z\sqrt{{K_{tc}}^2 + {K_{rc}}^2} \cdot Na_p + f_z\sqrt{{K_{tc}}^2 + {K_{rc}}^2} \cdot \sum_{j=1}^{N}\sum_{n=1}^{\infty}\left(\left(\left(\frac{a^*_{totn}}{nk_b}\sin nk_b a_p + \frac{b^*_{totn}}{nk_b}\cos nk_b a_p - \frac{b^*_{totn}}{nk_b}\right)\cos n\phi_j + \left(-\frac{a^*_{totn}}{nk_b}\cos nk_b a_p + \frac{a^*_{totn}}{nk_b} + \frac{b^*_{totn}}{nk_b}\sin nk_b a_p\right)\sin n\phi_j\right)\right) \quad (28)$$

Moreover, considering a force signal without tool run-out, it is also possible to remove the summation related to the number of flutes (N), simplifying the formulation in equation 28 as:

$$F_{tot}(\phi) = a^{**}_{tot0} \cdot f_z\sqrt{{K_{tc}}^2 + {K_{rc}}^2} \cdot Na_p + N \cdot f_z\sqrt{{K_{tc}}^2 + {K_{rc}}^2} \cdot \sum_{n}^{\infty}\left(\left(\left(\frac{a^*_{totn}}{nk_b}\sin nk_b a_p + \frac{b^*_{totn}}{nk_b}\cos nk_b a_p - \frac{b^*_{totn}}{nk_b}\right)\cos n\phi_j + \left(-\frac{a^*_{totn}}{nk_b}\cos nk_b a_p + \frac{a^*_{totn}}{nk_b} + \frac{b^*_{totn}}{nk_b}\sin nk_b a_p\right)\sin n\phi_j\right)\right) \quad n = N, 2N, .., \infty \quad (29)$$

In this case the Fourier series is not evaluated at each n-multiple of the rotational frequency but only at the ones divisible for N, hence related only to the tooth pass frequency.
FFT components for total force using the proposed simplifications become:

- For the constant term (null frequency):

$$A_0 = a^{**}_{tot0} \cdot f_z\sqrt{{K_{tc}}^2 + {K_{rc}}^2} \cdot Na_p \quad (30)$$

- For tooth pass frequency and its harmonics:

$$C_n = \frac{1}{2}N \cdot f_z\sqrt{{K_{tc}}^2 + {K_{rc}}^2} \cdot \left(\left(\frac{a^{**}_{totn}}{nk_b}\sin\left(nk_b a_p\right) + \frac{b^{**}_{totn}}{nk_b}\cos\left(nk_b a_p\right) - \frac{b^*_{x,yn}}{nk_b}\right) - i\left(-\frac{a^{**}_{totn}}{nk_b}\cos\left(nk_b a_p\right) + \frac{a^{**}_{totn}}{nk_b} + \frac{b^{**}_{totn}}{nk_b}\sin\left(nk_b a_p\right)\right)\right) \quad n = N, 2N, .., \infty \quad (31)$$

2.2 Depths of cut estimation

The proposed equations show that the ratios between C_n and A_0, called here R_n, are independent from the cutting force coefficients and the feed per tooth, but they depend only on tool properties (D, N, α_{hel}) and depths of cut (a_p, a_r), as shown in eq. 32:

$$R_n = \frac{C_n}{A_o} = \frac{1}{a_p a^{**}_{tot0}}\left(\left(\frac{a^{**}_{totn}}{nk_b}\sin\left(nk_b a_p\right) + \frac{b^{**}_{totn}}{nk_b}\cos\left(nk_b a_p\right) - \frac{b^*_{x,yn}}{nk_b}\right) - i\left(-\frac{a^{**}_{totn}}{nk_b}\cos\left(nk_b a_p\right) + \frac{a^{**}_{totn}}{nk_b} + \frac{b^{**}_{totn}}{nk_b}\sin\left(nk_b a_p\right)\right)\right) \quad (32)$$

The proposed monitoring solution will, hence, be based on this parameter. Since R_n is a complex number, both real and imaginary parts will be considered. During the identification procedure, the predicted R_n is compared to the experimental one to estimate the process depths of cut. To achieve such result, an optimization algorithm is implemented with the aim of minimizing the following error function f_o:

$$f_o = \frac{\left\|R_{np} - R_{nm}\right\|^2}{\|R_{nm}\|^2} \qquad n = 2,3, \dots, c \quad (33)$$

where c is the number of Fourier coefficients considered in the optimization, R_{np} and R_{nm} are the predicted and measured values of the ratio formulated in eq. 32. and || is the 2-norm of the vector.

2.3 Run-out removal

The proposed approach is based on cutting force signals analysis in the frequency domain. The analysis is focused on tooth pass frequency and its harmonics, thus neglecting tool run-out, generally significant in actual operations. However, it is possible, starting from cutting force signals generated

by a tool characterized by run-out, to compute the cutting forces that the same tool without run-out would generate.
In this work run-out is removed by means of a simple procedure that requires spindle speed value, summarized in these points:

- Cutting force signal is acquired and re-sampled to match a tooth pass period (i.e., sampling frequency multiple of the tooth pass frequency);
- Signal is analyzed considering a rotational period.
- The N-tooth pass periods included in the analyzed signal are averaged.
- The proposed approach is applied on the averaged tooth pass period.

The proposed procedure in time-domain, can be seen essentially as considering only tooth pass frequency and its harmonics on the cutting force signal in frequency domain, neglecting/removing the contributions of run-out frequency (i.e., rotational frequency and its harmonics). This is an interesting aspect, since in the future real-time implementation the run-out removal procedure could be re-arranged by just considering tooth pass frequency and harmonics of the force signal.
The proposed removal approach is valid both in case of low value of tool run-out, commonly found in actual milling tools, not causing any flute to be excluded by the cutting and also in case of high value of tool run-out, that causes some flutes to not be cut.
An example of such scenarios is presented in Fig. 2, where the results of two simulations are presented. The simulations were carried out considering a 4-fluted tool of 12 mm (45° helix angle) cutting Aluminum with 4 mm axial and 3 mm radial depths of cut (spindle speed 6366 rpm and 0.1 mm feed per tooth). The first simulation considers the tool with low run-out (0.015 mm) and the second one with a run-out higher than feed per tooth (0.15 mm). Simulated total force signals in presence of run-out were compared with no run-out simulation results and the signal obtained by applying the proposed run-out removal approach. As clear from the results (Fig. 2), the simple procedure proposed is effective in reproducing the no run-out condition starting from cutting force in presence of tool run-out.

2.4 Optimization algorithm

In order to estimate depths of cut, an optimization algorithm should be implemented to minimize the objective function presented in eq. 33. In this work a global constrained optimization algorithm is preferred to find a global optimal solution within feasible values of depths of cut. In particular, a genetic algorithm is adopted here. Genetic algorithms are efficient optimization algorithms based on the mechanics of natural genetics. Their "survival-of-the-fittest" approach allows them to perform a fitting procedure in a very efficient way compared to more-conventional search techniques [30]. It is worth to point out that genetic algorithm is implemented in this work to validate the proposed depths of cut identification strategy based on frequency ratio. However, this would not probably be the best solution for the future monitoring implementation, for which the most suitable algorithm for a real-time application should be defined and evaluated.
The implemented algorithm searches the best values of axial and radial depths of cut that minimizes the error function (f_o). In addition to depths of cut, phase shift is also considered. Indeed, since complex numbers are considered, phase shift between measured and predicted signals is very important for an accurate estimation of the parameters.

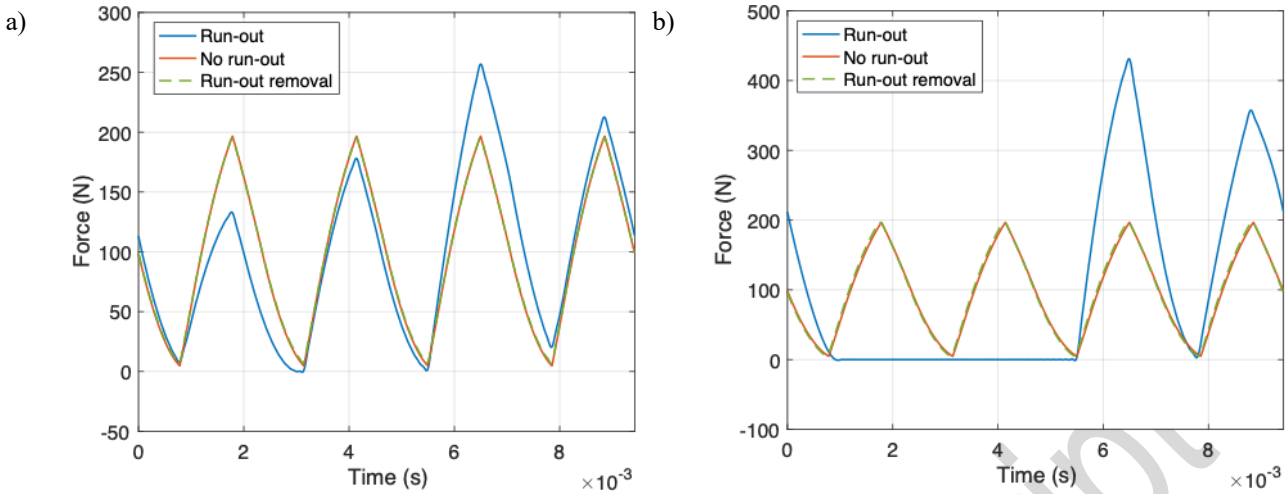

Fig. 2 Example of run-out removal results a) 0.015 mm run-out b) 0.15 mm run-out

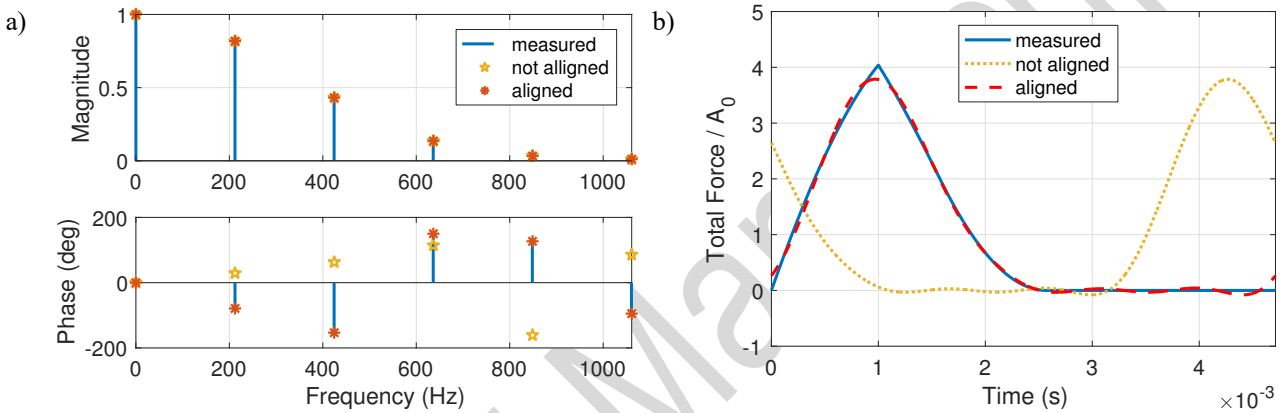

Fig. 3 Example of alignment between signals a) frequency domain b) time domain in the tooth pass interval

Therefore, the alignment of the two signals to be compared is essential. This aspect is exemplified in Fig. 3, where a measured signal is compared with two predicted signals (c=5), equal in shape but different in phase shift.

As shown in the figure, in case of the not aligned signal, results both in terms of frequency and time domain are not accurate (Fig. 3a) because of phase difference, while once the two signals are aligned the results are in good agreement. Magnitude is not affected by the shift; however, magnitude is not sufficient to perform a robust identification, since it does not ensure univocal results (i.e., the same normalized magnitude can be obtained by different cutting parameters).

To tackle this issue an additional parameter is added to the optimization: θ that represents the phase shift (rad) of the measured signal respect to the predicted one, and it is included using eq. 34:

$$C_{nshifted} = C_n * i^{n\frac{2\theta}{\pi}} \qquad 0 < \theta < 2\pi \qquad n = N, 2N, .., \infty \qquad (34)$$

In summary, three outputs are extracted by the proposed method:

1. radial depth of cut (a_r);
2. axial depth of cut (a_p);
3. phase shift (θ);

while the inputs required are:

- Measured cutting force on the x-y plane;
- Tool characteristics: diameter, number of flutes, helix angle;
- Spindle speed, that can also be extracted directly by the value of the tooth pass frequency found in the force spectrum, as in other works [15].

The strengths of the proposed method are:

- Relying on just cutting force signals, that could be acquired by commercial systems without the need of specific instrumentations.
- Not requiring any information on cutting force coefficients, since it is based on dimensionless cutting force (i.e., ratio between frequency contents and constant force term).
- Not requiring the knowledge about tool-run-out or tool direction of the cutting.

Therefore, a force-based cutting condition monitoring system based on the proposed approach could be easily implemented in an industrial environment.
On the other hand, one of the main limitations of the proposed approach is related to the accuracy of the cutting force measurement. Indeed, as previously mentioned, dynamometers are influenced by system dynamics and can return distorted results, especially in case of high spindle speed and low rigidity of workpiece (in case of table dynamometers) or tool (in case of rotating dynamometers). Several methods have been proposed in literature to compensate for such distortions, and/or improve measurement system dynamics.
The other limitations of the approach are associated to the approximations adopted in deriving eq. 32:

- The solution applies only to 2.5 axis end-milling.
- The method is proposed for flat end-mills, even if a similar approach based on different tool geometries could be developed.
- The method is effective in milling processes where cutting forces can be accurately represented by a lumped shear cutting force model.

It must be pointed out that this last assumption is valid even in case of varying force coefficients with cutting parameters. Therefore, this condition should be considered valid in several scenarios, as discussed in [17].

3. NUMERICAL VALIDATION

Firstly, the proposed approach and formulations presented in section 2 were tested using numerical validation. A series of time-domain simulation were carried out using the cutting force model in eq. 1-2. Discrete Fast Fourier Transformation (DFFT) was then applied to simulated total cutting forces on the x-y plane to compute the spectra of the cutting forces in frequency domain. The derived DFFT of the forces were then compared with the analytical formulations proposed. In addition, the proposed depth of cut estimation solution is applied to the signals, following the steps proposed in the previous section. This numerical validation allows us to test the proposed formulations and techniques in a controlled environment, validating the theory behind the method and estimating the intrinsic errors. For the optimization, a genetic algorithm with 3000 Population 3000 15 Generations was adopted to minimize the error function in eq. 33 and estimate the best depths of cut and shift angle. The range of parameters for the three variables are presented in Table 1. Only five Fourier coefficients were considered in the optimization (i.e., c=5).

Table 1. Optimization algorithm boundaries

Variable	Min	Max
a_p (mm)	0	30
a_r (mm)	0	D
θ	0	2π

Several tests were performed to investigate the proposed analytical expressions in different conditions, with the same spindle speed and feed per tooth, 6366 rpm and 0.1 mm respectively. The first simulation considers a 4-fluted 12 mm end-mill with 45° helix angle engaged 4 mm axially (a_p) and 3 mm in the radial direction (a_r). Starting from this condition, other simulations were carried out changing parameters (e.g., number of flutes, depths of cut, helix angle) to analyze their influence. Then, tests with the same engagement angles (α_{en}, α_{sw}) are analyzed (tests 10-11). Lastly, very small depths of cut (tests 12-13) and different materials (tests 14-15) were investigated. All the simulations were carried out in down-milling.

Cutting parameters used in the different simulations are summarized in Table 2, along with the results of the proposed solution. Cutting force coefficients adopted for the first 13 tests, typical of a 6082—T4 Aluminum [15], were K_{tc} 750 MPa and K_{rc} 150 MPa and for test 14 and 15 K_{tc} 2200 MPa and K_{rc} 750 MPa, typical of a carbon steel to check the behavior of the proposed approach with different materials.

Table 2. Cutting conditions numerically tested (spindle speed 6366 rpm and 0.1 mm feed per tooth)

ID	Material	D (mm)	N	α_{hel} (°)	commanded a_p (mm)	commanded a_r (mm)	estimated a_p (mm)	estimated a_r (mm)
1	Aluminum 6082-T4	12	4	45	4.00	3.00	4.00	3.00
2	Aluminum 6082-T4	12	2	45	4.00	3.00	4.01	3.00
3	Aluminum 6082-T4	12	6	45	4.00	3.00	4.00	2.99
4	Aluminum 6082-T4	12	4	25	4.00	3.00	4.03	2.98
5	Aluminum 6082-T4	12	4	50	4.00	3.00	4.02	2.99
6	Aluminum 6082-T4	12	4	45	2.00	3.00	1.99	3.01
7	Aluminum 6082-T4	12	4	45	10.00	3.00	9.99	3.00
8	Aluminum 6082-T4	12	4	45	4.00	1.00	4.00	1.00
9	Aluminum 6082-T4	12	4	45	4.00	9.00	4.01	9.01
10	Aluminum 6082-T4	12	4	20	10.99	3.00	11.06	2.97
11	Aluminum 6082-T4	20	4	45	6.67	5.00	6.68	4.97
12	Aluminum 6082-T4	12	4	45	1	0.5	0.99	0.50
13	Aluminum 6082-T4	12	4	45	0.1	0.2	0.10	0.20
14	Steel AISI-1045	12	4	45	4	3	4.00	3.00
15	Steel AISI-1045	12	4	45	0.1	0.2	0.10	0.20

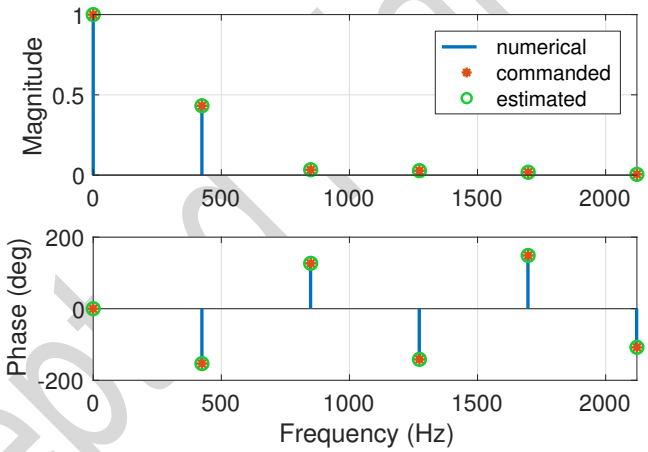

Fig. 4 Total cutting force spectrum for test 1

The results of the first test are reported in Fig. 4, where magnitude and phase of the FFT of total force divided by A_0 are shown. Using the formulation in section 2 spectrum of total forces is accurately predicted, proving the validity of the proposed formulations. Moreover, applying depth of cut identification algorithm based on f_o on the signal (without using the information of cutting force coefficients and depths of cut), the computed depths of cut (Table 2) are close to the ones imposed (error less than 1%). Similar trends can be found for all the numerical results.

In Fig. 5 the influence of the number of flutes of the tool is highlighted. As expected, increasing the number of flutes from 2 to 6 a reduction in significant harmonics is found. Indeed, increasing n the Fourier coefficients reduce their value (as clear from the equations in appendix A), and this apply also to N since it influences the coefficient number to be computed.

Fig. 5 confirms the accuracy of the proposed formulations and the same trend in the depth of cut estimation. This is valid also for the results shown in Fig. 6, where the helix angle of the tool is changed.

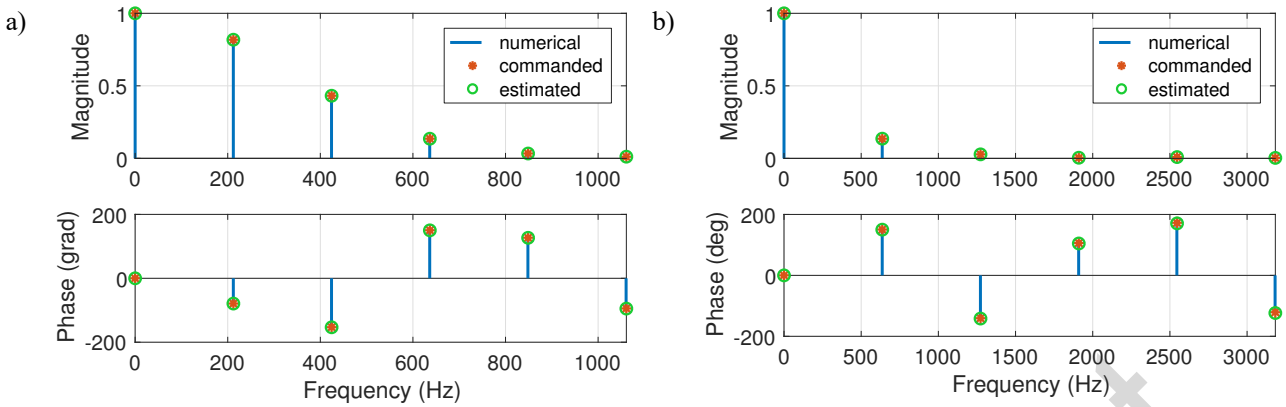

Fig. 5 Effects of number of flutes, total cutting force spectrum for a) test 2, N=2 b) test 3, N=6

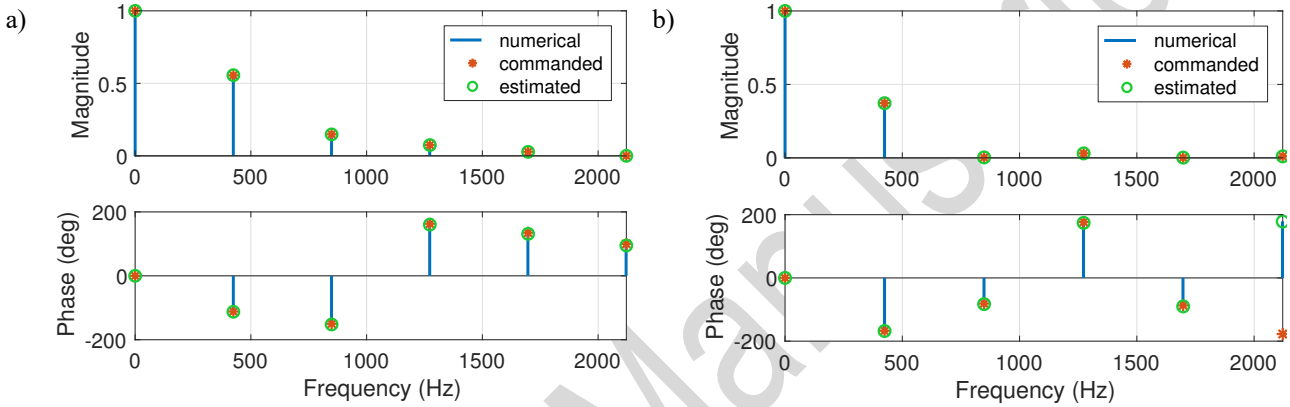

Fig. 6 Effects of helix angle, total cutting force spectrum for a) test 4, α_{hel}=25° b) test 5, α_{hel}=50°

Helix angle influences tooth pass frequency and its harmonics, indeed, looking at the proposed formulations, it affects α_{sw} and the shape of the force. Increasing the helix angle, the force is smoother, and the relevance of the harmonics is reduced.

In Fig. 7 the effect of axial depth of cut is shown, and the depths of cut estimated via optimization algorithm are still close to the simulated ones. Regarding the effect of axial depth of cut, an increase of the value leads to an increase of the constant term therefore the relevance of the tooth pass frequency and its harmonics diminished.

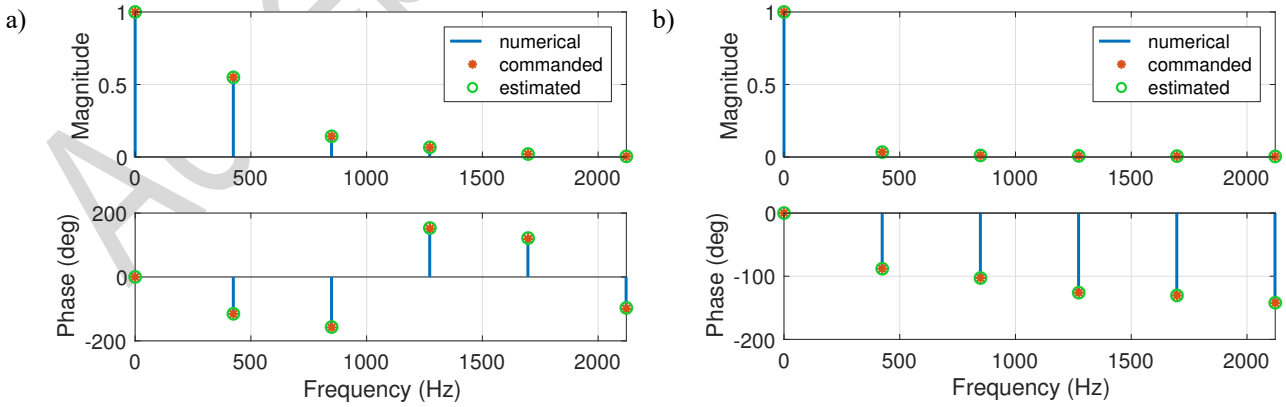

Fig. 7 Effects of axial depth of cut, total cutting force spectrum for a) test 6, a_p=2 b) test 7, a_p=10

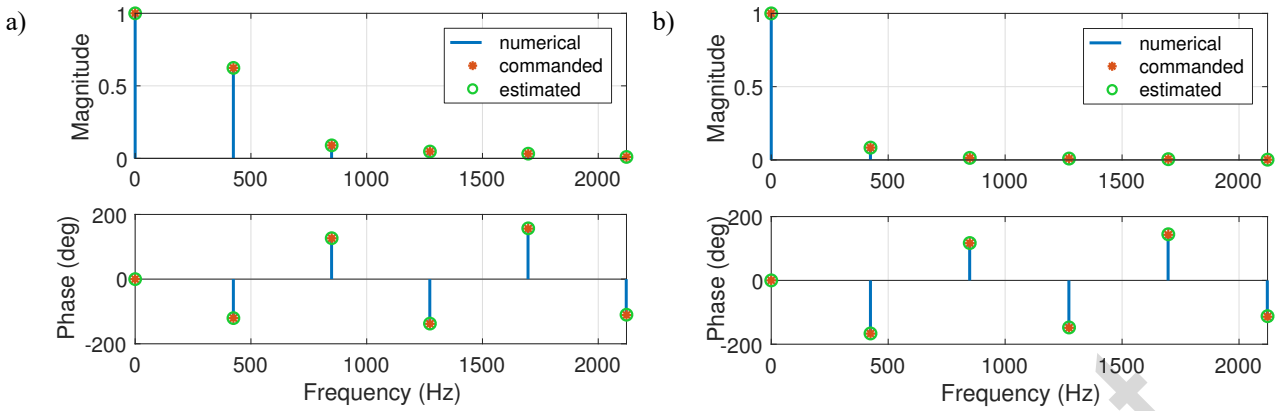

Fig. 8 Effects of radial depth of cut, total cutting force spectrum for a) test 8, a_r=1 b) test 9, a_r=9

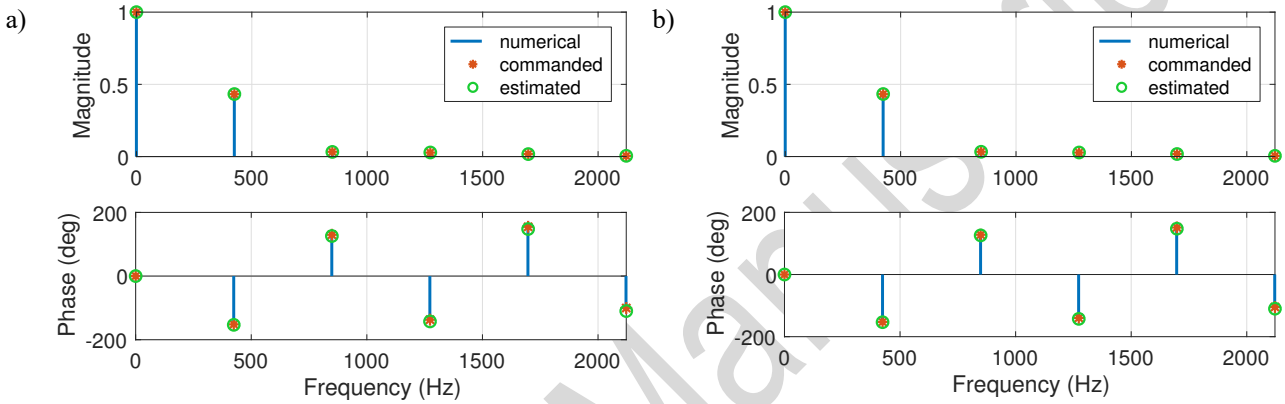

Fig. 9 Condition with the same α_{en} *and* α_{sw}*, total cutting force spectrum for a) test 10 b) test 11*

Similar considerations can be drawn for the radial depth of cut (Fig. 8). In addition to the analysis of the effects of the different parameters on the cutting forces spectra, two simulations were performed keeping constant the two engagement angles (α_{en}, α_{sw}), equal to the one of test 1 (Fig. 9). This is achieved by changing depths of cut and tool characteristics.

Results show that the spectra of the forces of test 10, 11 and 1 present the same distribution and the same ratios between the different components. This confirms that the engagement angles are important for the shape of the cutting forces. However, the proposed approach accurately estimates the depths of cut of the different tests since, although the same cutting force ratio are used as input, different tool characteristics are considered.

To further investigate low depths of cut, test 12 and 13 were performed and results provided in Fig. 10. In case of very low depths of cut, frequency contribution of tooth pass frequency harmonics is significant, as expected. These tests confirm the proposed approach accuracy in estimating the commanded depths of cut.

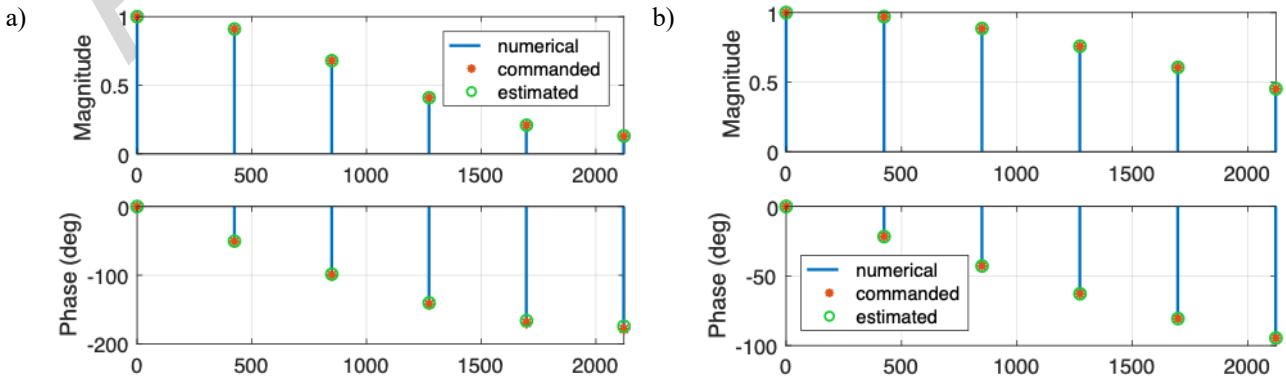

Fig. 10 Low depths of cut condition a) test 12 b) test 13

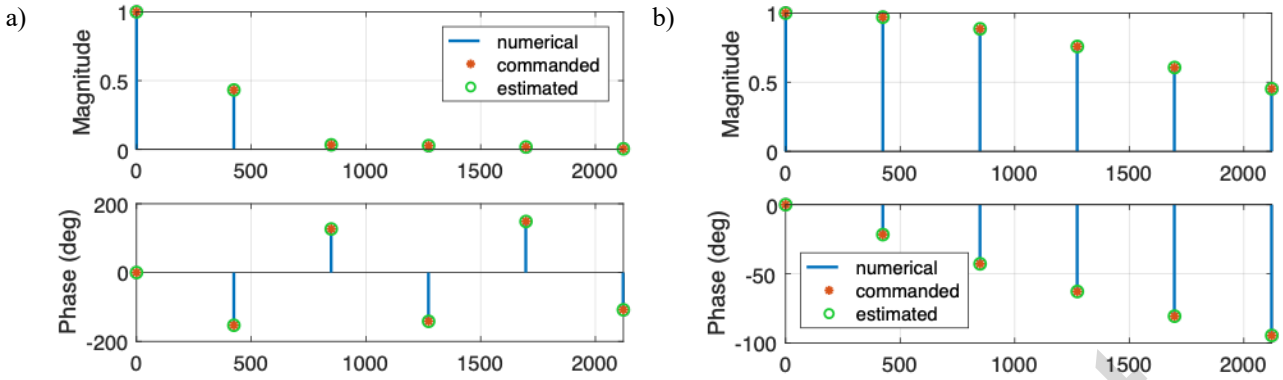

Fig. 11 Different material (steel) conditions a) test 14 b) test 15

In order to show the potentiality of the method to work on different material without the need of cutting force coefficients, test14 and test15 were simulated for carbon steel and results in terms of normalized FFT of the total cutting force are provided in Fig. 11. Results show that the proposed approach is able to accurately estimate depths of cut with different materials without the knowledge of cutting force coefficients. This is possible through the normalized frequency spectrum (R_n) that does not depend on material (i.e., cutting force coefficients) as long as a lumped shear force model is considered. This is clear by comparing two simulations that present the same parameters except for the material (test 1 and test 14): results of these simulations (Fig. 4 and Fig. 11a) show the same normalized FFT of total cutting force, confirming its independence on the material.
Fig. 12 summarizes the results of the identification procedure on the numerical validation. As clear from the figure, results show almost a perfect match between commanded and estimated values, confirming the validity of the theory on which the new monitoring system is based. The error found (Fig. 12b) are very low (less than 0.1 mm) and are probably related to the optimization algorithm effectiveness or to the time-domain simulation discretization that could introduce small errors in the actual frequency domain spectra.

4. EXPERIMENTAL VALIDATION

The proposed methodology was then validated on actual cutting force data, experimentally acquired. Five different cutting tests were performed on a DMG MORI DMU 75 milling machine on Aluminum (6082-T4) using a four-fluted end-mill (Garant 202552) with 12 mm diameter and 45° helix angle. During the tests, a Kistler 9257A table dynamometer was used to measure forces, its signals were acquired by an LMS Scadas at 102400 Hz sampling frequency. Feed per tooth was set to 0.1 mm, while two different spindle speeds were used (2191 rpm and 6366 rpm), and different engagement conditions were tested. Down-milling strategy was used. The proposed method was applied to the measured forces, as presented in section 3 for the simulated ones.

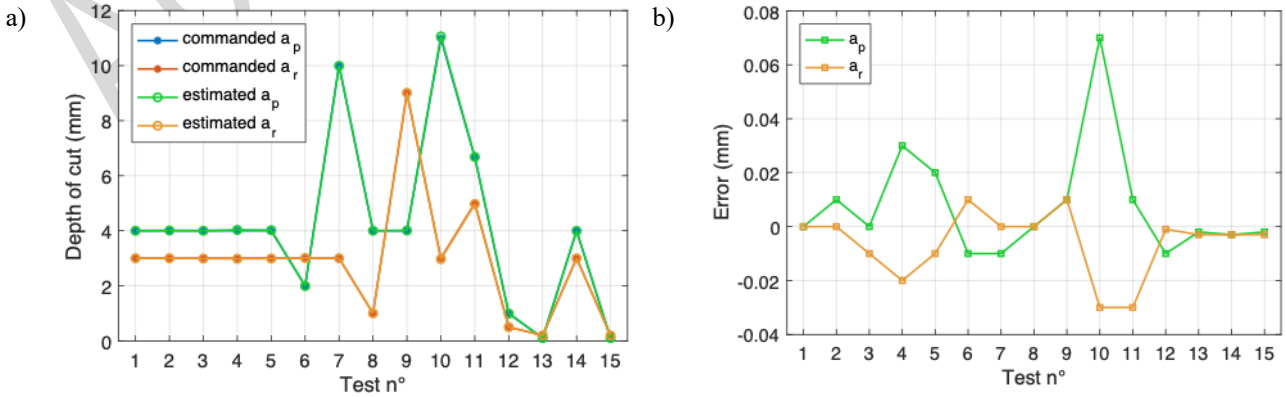

Fig. 12 Numerical validation results a) depths value b) error

Table 3. Cutting conditions experimentally tested (feed per tooth 0.1 mm)

ID	D (mm)	N	α_{hel} (°)	Spindle speed (rpm)	commanded a_p (mm)	commanded a_r (mm)	estimated a_p (mm)	estimated a_r (mm)
1	12	4	45	6366	1.00	6.00	1.25	6.29
2	12	4	45	2191	3.00	2.00	3.39	2.05
3	12	4	45	2191	8.00	2.00	7.74	2.25
4	12	4	45	2191	12.00	1.00	11.93	1.34
5	12	4	45	6366	15.00	2.50	15.21	2.66

Cutting parameters adopted are summarized in Table 3, where results in terms of estimated depths of cut are also reported. The acquired cutting forces were post-processed following the steps presented in section 2. Total force (i.e., resultant of cutting force in x-y plane) was computed by combining the forces measured by the dynamometer on the machine x-y plane. These forces were corrected to reduce the distortions derived by the system dynamics using the approach proposed by Scippa et al. [31], and post-processed to compensate for tool run-out as presented in the previous section. The same optimization algorithm presented in section 3 was used. Comparisons between measured force spectra (normalized to the constant force) and the proposed formulations, using both the commanded depths of cut and the ones obtained by the optimization algorithm, are presented in frequency and time domain in the following figures (Fig. 13, Fig. 14, Fig. 15, Fig. 16, Fig. 17).

In Fig. 13, the results for the experimental test with the lowest axial depth of cut (1 mm) and the highest radial depth of cut (6 mm, half-immersion) is presented. Good agreement is found on the frequency domain between measured signal and proposed formulations for both commanded and estimated depths (Fig. 13a). As expected, high accuracy is found also in the time-domain representation (Fig. 13b) both in terms of shape and alignment, confirming the good estimation of the phase shift (θ). Although the commanded and estimated depths of cut seem to provide very similar results, their values show some discrepancies. Indeed, both axial and radial depth of cut are overestimated by an amount of 0.3 mm with the proposed approach. This value, as absolute error, can be considered acceptable at least for some monitoring applications (e.g., detection of errors in programming, or collision), even if the relative error on axial depth of cut is high (25%).

For the results of the test 2 (Fig. 14), featuring low engagement conditions, similar considerations can be drawn. In this case, the tooth pass frequency is significant on the spectrum, exceeding half of the constant term and showing a highly intermittent cutting. Indeed, this cutting condition is characterized by only a single tooth engaged, as confirmed by the time-domain signal that presents a non-cutting zone (null force). Higher error is found for the axial depth of cut, while the estimation of the radial depth of cut is very accurate.

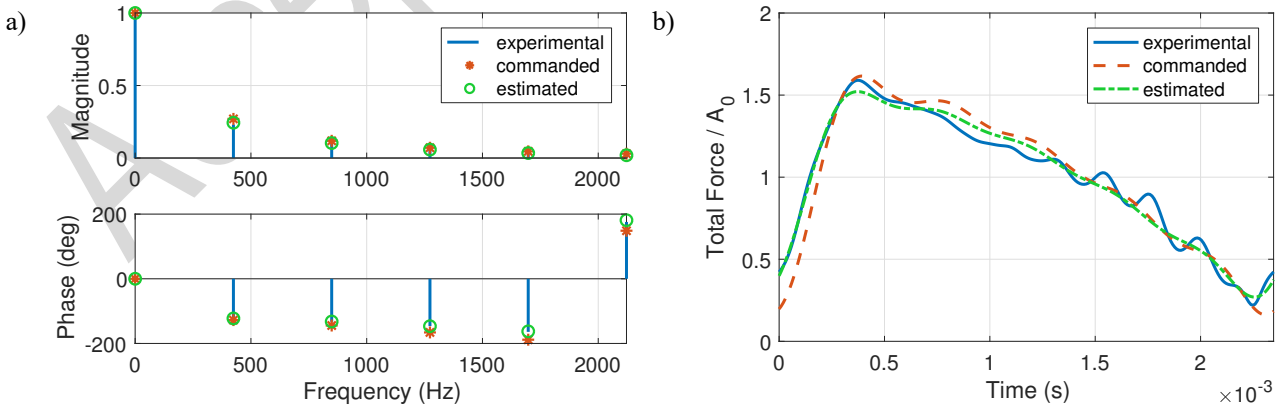

Fig. 13 Test 1 experimental cutting force, a) frequency domain b) time domain

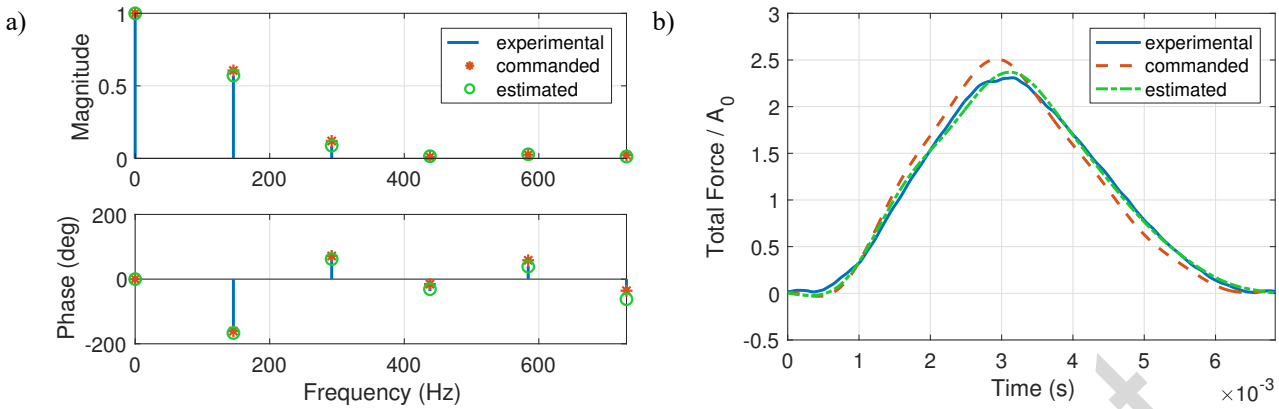

Fig. 14 Test 2 experimental cutting force, a) frequency domain b) time domain

Increasing a_p, tooth pass frequency magnitude respect to A_0 decreases (Fig. 15, Fig. 16, Fig. 17), as expected. These conditions are characterized by higher average forces that produce a flatter normalized shape, as it is clearly shown in the time-domain representation. Although cutting force shapes are different in the three cases, the proposed frequency domain formulations accurately predict the spectra with small deviations (more significant in phase) and the proposed method estimates depths of cut with a good accuracy.

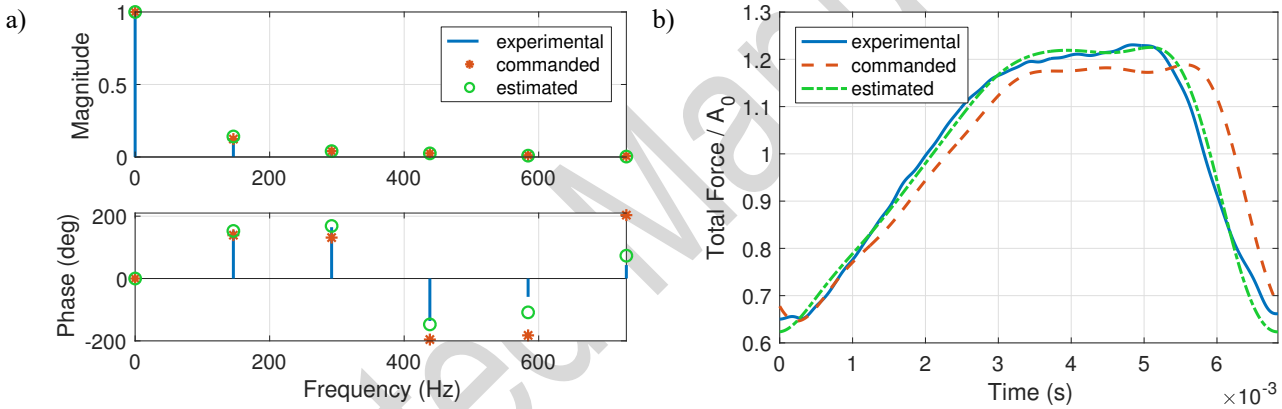

Fig. 15 Test 3 experimental cutting force, a) frequency domain b) time domain

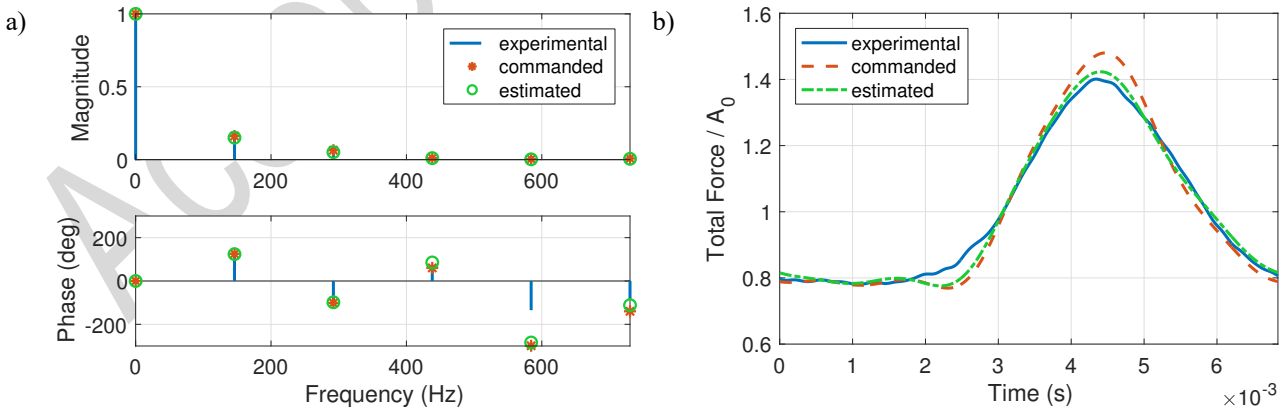

Fig. 16 Test 4 experimental cutting force, a) frequency domain b) time domain

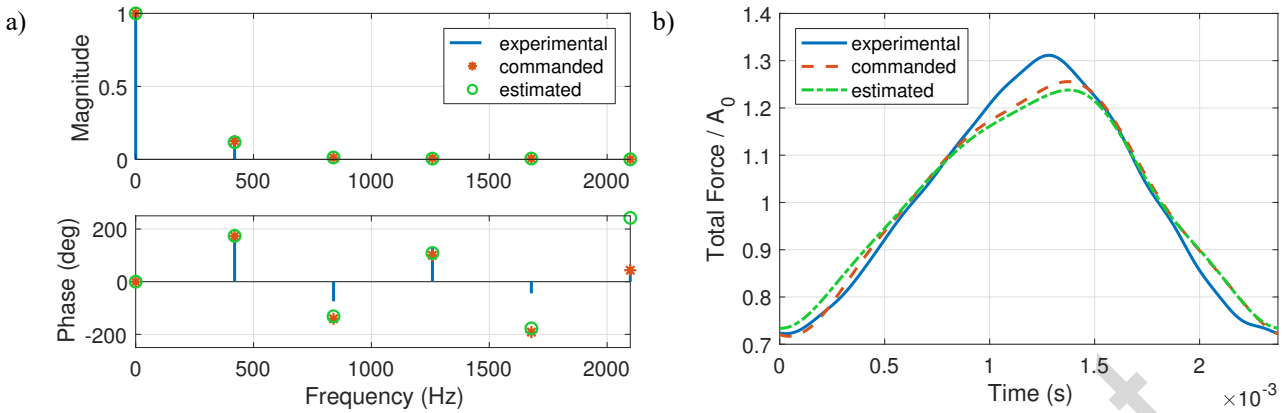

Fig. 17 Test 5 experimental cutting force, a) frequency domain b) time domain

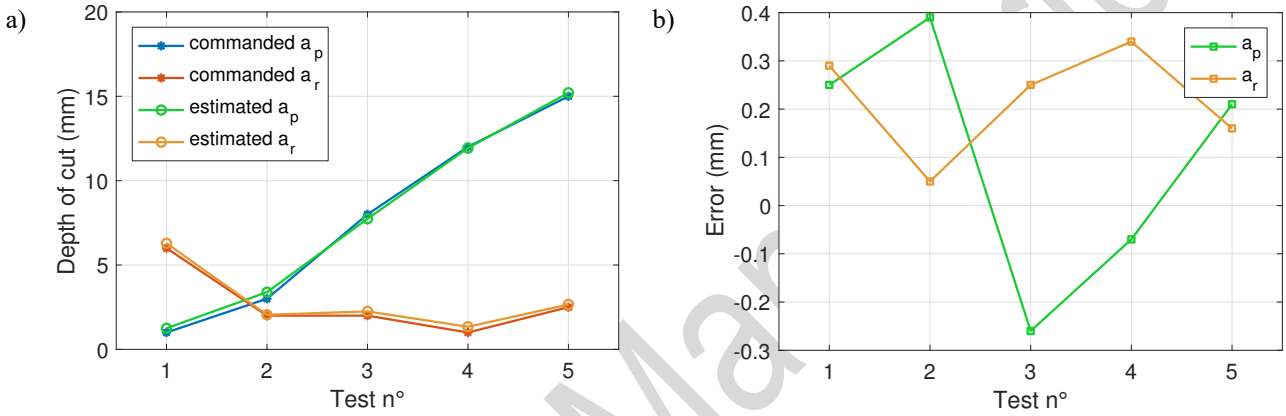

Fig. 18 Experimental validation results a) depths value b) errors

Focusing on the results of the proposed estimation approach, a summary of the depths of cut and absolute error for the five tests is presented in Fig. 18. As shown in the figure, commanded and estimated values are close for all the tests, with absolute error less than 0.4 mm for all the cases. Radial depth of cut is always overestimated, while axial depth of cut shows the higher error (both negative and positive). These discrepancies are due to the approximations of the method and to the uncertainties of the process and measurements. The first aspect includes the representation of the actual force with the lumped shear cutting force model, while the second aspect involves the errors in post-processing the measurements (e.g., dynamic compensation) and the actual depth of cut performed in the process, that could be different from the commanded ones. The identified accuracy is in line with other works in literature, such as the method proposed by Altintas et al. [18] that however requires calibration tests or the technique proposed by Prickett et al. [23] that has the limit of exploiting a dedicated instrumentation based on ultrasonic sensors. On the other hand, results are less accurate than the ones obtained by Leal-Munoz et al. [22], however their work has the drawbacks to be dedicated only to radial depth of cut and to be valid in specific cutting conditions (only one flute cutting simultaneously). The accuracy of the proposed approach could be considered sufficient for a monitoring solution able to prevent bad programming or toolpath deviations. More accurate identification requires additional efforts in improving the proposed approach to consider more complex cutting force models or optimization strategy. However, increasing the complexity of the approach could lead to affect some of its strengths, such as the independence of cutting force coefficients. Alternately, the depths of cut identification accuracy could be improved by combining the proposed approach with other solutions.

5. CONCLUSIONS

Cutting forces are one of the most significant signals for monitoring the milling process. Indeed, it presents peculiar characteristics that depend on several aspects, such as tool wear, cutting parameters, and they affect different process outcomes, such as machining error, vibrations.

In this work, the frequency content of the cutting forces (i.e., frequency spectrum) is analyzed and analytical formulations are proposed with the aim of developing a monitoring solution for depths of cut identification. Indeed, the real-time knowledge of both axial and radial depths of cut could be very useful in actual machining operations to prevent the tool from working out of the desired parameters, leading to machining errors or failures.

The main outcomes of this work are:

- The total force normalized spectrum respect to the constant term seems to be a promising parameter to be used for depths of cut monitoring.
- In the simplified conditions of a lumped shear cutting force model, the proposed normalized spectrum is independent of the cutting force coefficients and feed per tooth.
- The developed identification algorithm based on such a normalized spectrum does not require prior knowledge of cutting force coefficients or cutting directions, making it suitable for an industrial implementation.
- Analytical formulations for cutting force spectra were developed and numerically investigated, confirming their accuracy.
- A preliminary implementation of the proposed identification approach was validated on simulated and experimental cutting forces.
- The depths of cut identification returned accurate results on numerical and experimental validations, with absolute errors less than 0.4 mm on the estimated depths on experimental cutting forces.

The order of magnitude of such error is very promising since, if confirmed, could be low enough to exploit the proposed method for an accurate monitoring of engagement conditions suitable for many applications (e.g., prevent programming error or toolpath deviations).

The proposed approach is characterized by several interesting features:

- It uses cutting force signals that could be acquired by commercial systems without the need of specific instrumentations.
- It is based on a few frequency coefficients, derived by a frequency analysis of the signal, hence it is robust to noise.
- Cutting force coefficients are not required, since the method is based on dimensionless cutting force (i.e., ratio between frequency contents and constant force term).
- It does not require the knowledge about tool-run-out or tool direction of the cutting.

The proposed approach still presents some limitations and criticalities that must be tackled:

- The proposed approach effectiveness depends on the accuracy of the acquired cutting forces that can be distorted by system dynamics and must be corrected.
- The solution applies only to 2.5 axis end-milling.
- The method is proposed for flat end-mills, even if a similar approach based on different tool geometries could be developed.
- The method is effective in milling processes where cutting forces can be accurately represented by a lumped shear cutting force model.

A more robust approach should be developed, by considering a more complex cutting force model or coupling the proposed approach with other systems based on other parameters (e.g., force shape in time domain). Moreover, although the implementation of the frequency domain analysis increases the computational efficiency of the method, it still requires a FFT analysis of the cutting force and its post-processing (including the required dynamic compensation) that should be improved to be implemented in real-time. On the other hand, a frequency analysis of cutting force signals is adopted in other applications and can be coupled with the proposed approach. In particular it is worth to notice

that the proposed approach could be combined with a chatter detection approach based on frequency analysis to return both engagement conditions (i.e., depths of cut) and the occurrence of chatter, since generally chatter detection technique are based on chatter frequency identification that does not affect tooth pass frequency and harmonics. This combination is very interesting since the knowledge of depths of cut, spindle speed and presence of chatter vibrations could be exploited to automatically create a stability map (i.e., stability lobe diagrams) of the investigated tool during actual operations without the need of tailored experimental procedures.

Author Contributions: Conceptualization and Methodology N.G., L.M..; Investigation and Validation N.G., L.M.; Writing - Original Draft N.G.; Writing – Review & Editing, A.S., L.M.; Supervision A.S., G.C.; Project administration and Funding acquisition, G.C.

Funding: The research received no external funding.

Data Availability Statement: No data are available but can be provided upon request.

Acknowledgments: The authors would like to thank Machine Tool Technology Research Foundation (MTTRF) and its supporters for the loaned machine tool (DMG MORI DMU 75 MonoBlock).

Conflicts of Interest: The authors declare no conflict of interest.

REFERENCES

[1] C. Ratnam, K. Arun Vikram, B.S. Ben, B.S.N. Murthy, Process monitoring and effects of process parameters on responses in turn-milling operations based on SN ratio and ANOVA, Meas. J. Int. Meas. Confed. 94 (2016) 221–232. doi:10.1016/j.measurement.2016.07.090.

[2] X. Zhang, T. Pan, A. Ma, W. Zhao, High efficiency orientated milling parameter optimization with tool wear monitoring in roughing operation, Mech. Syst. Signal Process. 165 (2022) 108394. doi:10.1016/j.ymssp.2021.108394.

[3] G. Totis, O. Adams, M. Sortino, D. Veselovac, F. Klocke, Development of an innovative plate dynamometer for advanced milling and drilling applications, Meas. J. Int. Meas. Confed. 49 (2014) 164–181. doi:10.1016/j.measurement.2013.11.049.

[4] D. Kim, D. Jeon, Fuzzy-logic control of cutting forces in CNC milling processes using motor currents as indirect force sensors, Precis. Eng. 35 (2011) 143–152. doi:10.1016/j.precisioneng.2010.09.001.

[5] G. Totis, M. Sortino, Upgraded Regularized Deconvolution of complex dynamometer dynamics for an improved correction of cutting forces in milling, Mech. Syst. Signal Process. 166 (2022) 108412. doi:10.1016/j.ymssp.2021.108412.

[6] D. Richiedei, Adaptive shaper-based filters for fast dynamic filtering of load cell measurements, Mech. Syst. Signal Process. 167 (2022) 108541. doi:10.1016/j.ymssp.2021.108541.

[7] C. Wang, X. Zhang, B. Qiao, X. Chen, H. Cao, Milling force identification from acceleration signals using regularization method based on TSVD in peripheral milling, Procedia CIRP. 77 (2018) 18–21. doi:10.1016/j.procir.2018.08.195.

[8] P. Albertelli, M. Goletti, M. Torta, M. Salehi, M. Monno, Model-based broadband estimation of cutting forces and tool vibration in milling through in-process indirect multiple-sensors measurements, Int. J. Adv. Manuf. Technol. 82 (2016) 779–796. doi:10.1007/s00170-015-7402-x.

[9] H. Mostaghimi, C.I. Park, G. Kang, S.S. Park, D.Y. Lee, Reconstruction of cutting forces through fusion of accelerometer and spindle current signals, J. Manuf. Process. 68 (2021) 990–1003. doi:10.1016/j.jmapro.2021.06.007.

[10] G. Urbikain Pelayo, D. Olvera Trejo, Model-based phase shift optimization of serrated end mills: Minimizing forces and surface location error, Mech. Syst. Signal Process. 144 (2020) 106860. doi:10.1016/j.ymssp.2020.106860.

[11] S. Wojciechowski, M. Matuszak, B. Powałka, M. Madajewski, R.W. Maruda, G.M. Królczyk, Prediction of cutting forces during micro end milling considering chip thickness accumulation, Int. J. Mach. Tools Manuf. 147 (2019). doi:10.1016/j.ijmachtools.2019.103466.

[12] S. Wojciechowski, The estimation of cutting forces and specific force coefficients during finishing ball end milling of inclined surfaces, Int. J. Mach. Tools Manuf. 89 (2015) 110–123. doi:10.1016/j.ijmachtools.2014.10.006.

[13] H. Perez, E. Diez, J.J. Marquez, A. Vizan, An enhanced method for cutting force estimation in peripheral milling, Int. J. Adv. Manuf. Technol. 69 (2013) 1731–1741. doi:10.1007/s00170-013-5153-0.

[14] E. Ducroux, G. Fromentin, F. Viprey, D. Prat, A. D'Acunto, New mechanistic cutting force model for milling additive manufactured Inconel 718 considering effects of tool wear evolution and actual tool geometry, J. Manuf.

Process. 64 (2021) 67–80. doi:10.1016/j.jmapro.2020.12.042.
[15] N. Grossi, Accurate and fast measurement of specific cutting force coefficients changing with spindle speed, Int. J. Precis. Eng. Manuf. 18 (2017). doi:10.1007/s12541-017-0137-x.
[16] S. Wojciechowski, R.W. Maruda, P. Nieslony, G.M. Krolczyk, Investigation on the edge forces in ball end milling of inclined surfaces, Int. J. Mech. Sci. 119 (2016) 360–369. doi:10.1016/j.ijmecsci.2016.10.034.
[17] J.J.J. Wang, H.C. Chang, Extracting cutting constants via harmonic force components for a general helical end mill, Int. J. Adv. Manuf. Technol. 24 (2004) 415–424. doi:10.1007/s00170-003-1664-4.
[18] Y. Altintas, I. Yellowley, The identification of radial width and axial depth of cut in peripheral milling, Int. J. Mach. Tools Manuf. 27 (1987) 367–381. doi:https://doi.org/10.1016/S0890-6955(87)80010-X.
[19] J.G. Choi, M.Y. Yang, In-process prediction of cutting depths in end milling, Int. J. Mach. Tools Manuf. 39 (1999) 705–721. doi:10.1016/S0890-6955(98)00067-4.
[20] L. Yang, R.E. DeVor, S.G. Kapoor, Analysis of force shape characteristics and detection of depth-of-cut variations in end milling, J. Manuf. Sci. Eng. Trans. ASME. 127 (2005) 454–462. doi:10.1115/1.1947207.
[21] E. Leal-Muñoz, E. Diez, H. Perez, A. Vizan, Identification of the Actual Process Parameters for Finishing Operations in Peripheral Milling, J. Manuf. Sci. Eng. Trans. ASME. 140 (2018) 1–7. doi:10.1115/1.4039917.
[22] E. Leal-Muñoz, E. Diez, H. Perez, A. Vizan, Accuracy of a new online method for measuring machining parameters in milling, Meas. J. Int. Meas. Confed. 128 (2018) 170–179. doi:10.1016/j.measurement.2018.06.018.
[23] P.W. Prickett, R.A. Siddiqui, R.I. Grosvenor, The development of an end-milling process depth of cut monitoring system, Int. J. Adv. Manuf. Technol. 52 (2011) 89–100. doi:10.1007/s00170-010-2711-6.
[24] H. Gaja, F. Liou, Automatic detection of depth of cut during end milling operation using acoustic emission sensor, Int. J. Adv. Manuf. Technol. 86 (2016) 2913–2925. doi:10.1007/s00170-016-8395-9.
[25] J.J. Junz Wang, C.M. Zheng, An analytical force model with shearing and ploughing mechanisms for end milling, Int. J. Mach. Tools Manuf. 42 (2002) 761–771. doi:https://doi.org/10.1016/S0890-6955(02)00019-6.
[26] J.J.J. Wang, C.M. Zheng, Identification of cutter offset in end milling without a prior knowledge of cutting coefficients, Int. J. Mach. Tools Manuf. 43 (2003) 687–697. doi:10.1016/S0890-6955(03)00028-2.
[27] D. Bachrathy, J. Munoa, G. Stepan, Experimental validation of appropriate axial immersions for helical mills, Int. J. Adv. Manuf. Technol. 84 (2016) 1295–1302. doi:10.1007/s00170-015-7748-0.
[28] T.L. Schmitz, B.P. Mann, Closed-form solutions for surface location error in milling, Int. J. Mach. Tools Manuf. 46 (2006) 1369–1377. doi:http://dx.doi.org/10.1016/j.ijmachtools.2005.10.007.
[29] E. Budak, Y. Altintaş, Analytical Prediction of Chatter Stability in Milling—Part I: General Formulation, J. Dyn. Syst. Meas. Control. 120 (1998) 22. doi:10.1115/1.2801317.
[30] C.L. Karr, B. Weck, D.L. Massart, P. Vankeerberghen, Least median squares curve fitting using a genetic algorithm, Eng. Appl. Artif. Intell. 8 (1995) 177–189. doi:http://dx.doi.org/10.1016/0952-1976(94)00064-T.
[31] A. Scippa, L. Sallese, N. Grossi, G. Campatelli, Improved dynamic compensation for accurate cutting force measurements in milling applications, Mech. Syst. Signal Process. 54 (2015) 314–324. doi:10.1016/j.ymssp.2014.08.019.

APPENDIX A

The coefficients for the Fourier series computation of cutting forces are provided here.

$$a^*_{tot0} = -\frac{1}{2\pi} f_z \sqrt{{K_{tc}}^2 + {K_{rc}}^2} [(\cos(x))]_{\phi_{in}}^{\phi_{out}} \quad (A.1)$$

$$a^*_{tot1} = -\frac{1}{\pi} f_z \sqrt{{K_{tc}}^2 + {K_{rc}}^2} [\left(\frac{1}{4}\cos(2x)\right)]_{\phi_{in}}^{\phi_{out}} \quad (A.2)$$

$$a^*_{totj} = -\frac{1}{\pi} f_z \sqrt{{K_{tc}}^2 + {K_{rc}}^2} [\left(-\frac{1}{2(j-1)}\cos\left((j-1)x\right) + \frac{1}{2(j+1)}\cos\left((j+1)x\right)\right)]_{\phi_{in}}^{\phi_{out}} \quad (A.3)$$

$$b^*_{tot1} = -\frac{1}{\pi} f_z \sqrt{{K_{tc}}^2 + {K_{rc}}^2} [\left(-\frac{x}{2} + \frac{1}{4}\sin(2x)\right)]_{\phi_{in}}^{\phi_{out}} \quad (A.4)$$

$$b^*_{totj} = -\frac{1}{\pi} f_z \sqrt{{K_{tc}}^2 + {K_{rc}}^2} [\left(-\frac{1}{2(j-1)}\sin\left((j-1)x\right) + \frac{1}{2(j+1)}\sin\left((j+1)x\right)\right)]_{\phi_{in}}^{\phi_{out}} \quad (A.5)$$

$$a^{**}_{tot0} = -\frac{1}{2\pi} [(\cos(x))]_{\phi_{in}}^{\phi_{out}} \quad (A.6)$$

$$a^{**}_{tot1} = -\frac{1}{\pi} [\left(\frac{1}{4}\cos(2x)\right)]_{\phi_{in}}^{\phi_{out}} \quad (A.7)$$

$$a^{**}_{totj} = -\frac{1}{\pi} [\left(-\frac{1}{2(j-1)}\cos\left((j-1)x\right) + \frac{1}{2(j+1)}\cos\left((j+1)x\right)\right)]_{\phi_{in}}^{\phi_{out}} \quad (A.8)$$

$$b_{tot1}^{**} = -\frac{1}{\pi}\left[\left(-\frac{x}{2}+\frac{1}{4}\sin(2x)\right)\right]_{\phi_{in}}^{\phi_{out}} \quad \text{(A.9)}$$

$$b_{totj}^{**} = -\frac{1}{\pi}\left[\left(-\frac{1}{2(j-1)}\sin\big((j-1)x\big)+\frac{1}{2(j+1)}\sin\big((j+1)x\big)\right)\right]_{\phi_{in}}^{\phi_{out}} \quad \text{(A.10)}$$